Available online at www.sciencedirect.com
SCIENCE DIRECT®
Journal of Sound and Vibration 278 (2004) 257–283
JOURNAL OF SOUND AND VIBRATION
www.elsevier.com/locate/jsvi

Influence of active stiffening on dynamic behaviour of piezo-hygro-thermo-elastic composite plates and shells

S. Raja[a], P.K. Sinha[b,*], G. Prathap[c], D. Dwarakanathan[a]

[a] *Structures Division, National Aerospace Laboratories, Bangalore 560017, India*
[b] *Department of Aerospace Engineering, Indian Institute of Technology, Kharagpur 721302 (WB), India*
[c] *CSIR Center for Mathematical Modelling and Computer Simulation, Bangalore 560037, India*

Received 28 October 2002; accepted 6 October 2003

Abstract

The active stiffening and active compensation analyses are carried out to present the influence of active stiffness on the dynamic behaviour of piezo-hygro-thermo-elastic laminates. A coupled piezoelectric finite element formulation involving a hygrothermal strain field is derived using the virtual work principle and is employed in a nine-noded field consistent Lagrangian element. The closed-loop system is modelled with elastic stiffness, active stiffness introduced by isotropic actuator lamina and geometric stiffness due to stresses developed by hygrothermal strain. Through a parametric study, the influence of active stiffening and active compensation effects on the dynamics of cross-ply and angle-ply laminated plates and shells are highlighted. The active stiffening on thin shells is significantly influenced by boundary effects and the actuator efficiency further decreases with increase in curvature. The reduction in natural frequencies of cross-ply laminates due to hygrothermal strain is actively compensated by active stiffening; however, it is observed that the actuator performance reduces significantly with increase in curvature particularly in angle-ply laminates, which demands the use of directional actuators. The active stiffening and active compensation effects are low in moderately thick piezo-hygro-thermo-elastic plates and shells, which are less influenced by boundary conditions.

1. Introduction

Structural performance can be enhanced through active effects by applying smart concepts and this can provide controlled or desired responses within the flight spectrum of aerospace vehicles.

*Corresponding author. Tel.: +91-03222-83016; fax: +91-03222-55303, +91-03222-77190.
E-mail address: pksinha@aero.iitkgp.ernet.in (P.K. Sinha).

0022-460X/$ - see front matter © 2003 Elsevier Ltd. All rights reserved.
doi:10.1016/j.jsv.2003.10.002

Active materials make conventional composite structures smart or adaptive by adding multifunctional capabilities to output the necessary information about the change in structural characteristics during the operational conditions. The multifunctional piezoelectric materials employed in the vibration control applications respond to multifields such as electrical, thermal and mechanical.

Tzou and Ye [1], Lee and Saravanos [2] and Raja et al. [3] evaluated the thermal effect on piezoelectric coupling to show the importance of temperature-developed sensor voltage through thermal strain effect and electrothermal coupling. Influence of thermal strain was observed to be more significant than the electrothermal coupling on direct piezoelectric effect. Jonnalagadda et al. [4] and Blandford et al. [5] considered the thermal and electrical effects on elastic media as initial fields and developed the finite element (FE) procedures using first order shear deformation theory to analyze plates and beams. Chandrashekhara and Kolli [6] studied the thermomechanical dynamic response control of piezo-thermo-elastic composite shells by active effect. Lee and Saravanos [7] captured the sensory behaviour of piezo-thermo-elastic shell structures using FE analysis to show the electrothermal and electromechanical influence on sensor voltage.

Zhou et al. [8] developed a coupled thermo-piezoelectric-mechanical model using higher order laminate theory and higher order thermal field to study the response of composite plates. A significant difference was reported between the coupled and uncoupled models in predicting the piezo-thermo-elastic behaviour. Ishihara and Noda [9] obtained the analytical solutions considering shear deformation effect to predict the frequencies of piezo-thermo-elastic plates.

The thermal field influence on piezoelectric coupling has also received much attention from the control point of view in recent years. Tzou and Zhou [10] and Bao et al. [11] studied the static and dynamic control of laminated piezo-thermo-elastic beams, plates and shells with non-linear mathematical models. Oh et al. [12,13] investigated the post-buckling and vibration behaviour of piezoelectric laminated plates subjected to large thermal deflections. Shen and Kuang [14] proposed an analytical solution to solve the vibration control of simply supported piezo-thermo-elastic plate with velocity feedback.

The piezoelectric lamina as an actuator has the potential to modify the strain energy (active stiffening: displacement control) and damping (active damping: velocity control) of the structural system in a feedback control environment. The performance of the piezoelectric actuator system such as monolithic piezowafer (3–1, 3–2 actuation), piezofibre composite (PFC; 3–1 actuation) and active fibre composite (AFC; 3–3 actuation) may be influenced by hygrothermal strain. The hygral effect will be significant in AFC and PFC because the piezofibres are embedded in a polymer matrix. Therefore, a systematic assessment of active stiffening effect in controlling the vibration of piezo-hygro-thermo-elastic composite plates and shells is attempted to evaluate the performance of the piezoelectric lamina.

In the present paper, the influence of active stiffening on the frequency control of piezo-hygro-thermo-elastic laminated plates and shells are presented for various elastic modes. Active stiffening through actuation (piezoelectric) and active compensation through actuation (piezo-thermo-elastic and piezo-hygro-elastic) are studied on cross-ply and angle-ply laminates.

2. Basic equations and weak formulation

The constitutive equations of a piezo-hygro-thermo-elastic lamina can be expressed as

$$\sigma_{ij} = c_{ijkl}\varepsilon_{kl} - d_{kij}E_k - \lambda_{ij}T - \Lambda_{ij}\chi, \tag{1}$$

$$D_j = d_{jkl}\varepsilon_{kl} + \kappa_{jk}E_k + P_jT, \tag{2}$$

where $\sigma_{ij}, D_j, \varepsilon_{kl}, E_k, T$ and χ are the incremental stress, electric displacement, strain field, electric field, temperature and moisture, respectively. In the above equations, $c_{ijkl}, d_{kij}, \kappa_{jk}$ and P_j are the elastic, piezoelectric, dielectric and pyroelectric constants, respectively and $\lambda_{ij} = c_{ijkl}\alpha_{kl}$ is the thermoelastic constant and $\Lambda_{ij} = c_{ijkl}\beta_{kl}$ is the hygroelastic constant.

The final state of stress in the piezo-hygro-thermo-elastic system can be expressed as

$$\sigma^f_{ij} = \sigma_{ij} + \sigma^e_{ij}$$

where

$$\sigma_{ij} = \{\sigma_x, \sigma_y, \tau_{xy}, \tau_{xz}, \tau_{yz}\}^{\mathrm{T}},$$

$$\sigma^e_{ij} = \{\sigma^e_x, \sigma^e_y, \tau^e_{xy}, \tau^e_{xz}, \tau^e_{yz}\}^{\mathrm{T}}. \tag{3}$$

In Eq. (3), σ_{ij} are the incremental stresses and σ^e_{ij} are the stresses induced due to temperature and moisture. Note that the normal stress σ_z is assumed to be negligible.

The strain energy density in the piezo-hygro-thermo-elastic system can be expressed as

$$U_{PE} = \tfrac{1}{2}\sigma_{ij}\varepsilon_{ij} + \sigma^{\mathrm{e}}_{ij}\varepsilon_{ij}. \tag{4}$$

The non-linear strain–displacement relations are defined, following Lee and Yen [15], as

$$\varepsilon_{ij} = \varepsilon^l_{ij} + \varepsilon^{nl}_{ij}, \tag{5}$$

where $\varepsilon^l_{ij} = \{\varepsilon_{xx}, \varepsilon_{yy}, \gamma_{xy}, \gamma_{xz}, \gamma_{yz}\}^{\mathrm{T}}$ are the linear strains and $\varepsilon^{nl}_{ij} = \{\varepsilon^{nl}_{xx}, \varepsilon^{nl}_{yy}, \gamma^{nl}_{xy}, \gamma^{nl}_{xz}, \gamma^{nl}_{yz}\}^{\mathrm{T}}$ are the non-linear strains.

After substituting Eq. (5) into Eq. (4) and neglecting the higher order terms in displacement gradients ($\frac{1}{2}\sigma_{ij}\varepsilon^{nl}_{ij}$), we obtain

$$U_{PE} = \tfrac{1}{2}\sigma_{ij}\varepsilon^l_{ij} + \sigma^e_{ij}\varepsilon^l_{ij} + \sigma^e_{ij}\varepsilon^{nl}_{ij}. \tag{6}$$

The incremental potential energy in the system is obtained, following Lee and Yen [15], as

$$\Delta U_{PE} = U_{PE} - \sigma^e_{ij}\varepsilon^l_{ij},$$

$$\Delta U_{PE} = \tfrac{1}{2}\sigma_{ij}\varepsilon^l_{ij} + \sigma^e_{ij}\varepsilon^{nl}_{ij}. \tag{7}$$

The stress equation of motion is given by

$$\sigma^{f}_{ij,i} + f_{bj} = \rho \ddot{u}_j. \tag{8}$$

The virtual work done is thus derived for a piezo-hygro-thermo-elastic actuator, using Eqs. (7) and (8) and with the help of natural boundary condition $\sigma_{ij} n_i = f_{sj}$, as

$$\delta U_a = \int_v (\rho \ddot{u}_j \delta u_j + \sigma_{ij} \delta \varepsilon^{l}_{ij} + \sigma^{e}_{ij} \delta \varepsilon^{nl}_{ij}) \, \mathrm{d}v - \int_v (f_{bj} \delta u_j \, \mathrm{d}v) - \int_A (f_{sj} \delta u_j \, \mathrm{d}A), \tag{9}$$

where ρ, f_{bj} and f_{sj}, are density, body force and surface traction, respectively. The virtual work done is obtained for a piezo-hygro-thermo-elastic sensor, using the equation of electrostatics and with the help of natural boundary condition $D_i n_i = q$, as

$$\delta U_s = \int_v (D_j \delta \phi_{,j}) \, \mathrm{d}v - \int_s (q \delta \phi) \, \mathrm{d}s, \tag{10}$$

where ϕ and q are scalar electric potential and surface charge per unit area, respectively.

The generalized weak form of coupled piezo-hygro-thermo-elastic problem is then derived using Eqs. (1), (2), (9) and (10) as

$$\delta U_a + \delta U_s = 0,$$

$$\int_v [(\rho \ddot{u}_j \delta u_j) + (c_{ijkl} \varepsilon^{l}_{kl} \delta \varepsilon^{l}_{ij}) - (d_{kij} E_k \delta \varepsilon^{l}_{ij}) - (d_{jkl} \varepsilon^{l}_{kl} \delta E_j) - (\kappa_{jk} E_k \delta E_j)] \, \mathrm{d}v + \int_v \sigma^{e}_{ij} \delta \varepsilon^{nl}_{ij} \, \mathrm{d}v$$
$$= \int_v [(\lambda_{ij} T \delta \varepsilon^{l}_{ij}) + (\Lambda_{ij} \chi \delta \varepsilon^{l}_{ij}) - (P_j T \delta E_j)] \, \mathrm{d}v + \int_s f_{sj} \delta u_j \, \mathrm{d}s + \int_s q \delta \phi \, \mathrm{d}s, \tag{11}$$

where the body force is not considered in the present formulation.

3. Lamina constitutive equation

The lamina is assumed as elastically orthotropic and piezoelectrically orthorhombic crystal class mm2. The constitutive relation of an active lamina with respect to X–Y–Z co-ordinate system is given by

$$\begin{Bmatrix} \sigma \\ D \end{Bmatrix}_{xyz} = [\bar{Q}] \begin{Bmatrix} \varepsilon \\ E \end{Bmatrix}_{xyz},$$

where $[\bar{Q}] = [T]^{\mathrm{T}}[Q][T]$, T is the transformation matrix and

$$\begin{Bmatrix} \sigma_x \\ \sigma_y \\ \tau_{xy} \\ \tau_{yz} \\ \tau_{xz} \\ D_x \\ D_y \\ D_z \end{Bmatrix} = \begin{bmatrix} \bar{Q}_{11} & \bar{Q}_{12} & \bar{Q}_{16} & 0 & 0 & 0 & 0 & \bar{Q}_{PE31} \\ \bar{Q}_{12} & \bar{Q}_{22} & \bar{Q}_{26} & 0 & 0 & 0 & 0 & \bar{Q}_{PE32} \\ \bar{Q}_{16} & \bar{Q}_{26} & \bar{Q}_{66} & 0 & 0 & 0 & 0 & \bar{Q}_{PE36} \\ 0 & 0 & 0 & \bar{Q}_{44} & \bar{Q}_{45} & \bar{Q}_{PE14} & \bar{Q}_{PE24} & 0 \\ 0 & 0 & 0 & \bar{Q}_{45} & \bar{Q}_{55} & \bar{Q}_{PE15} & \bar{Q}_{PE25} & 0 \\ 0 & 0 & 0 & \bar{Q}_{PE14} & \bar{Q}_{PE15} & \bar{Q}_{DE11} & 0 & 0 \\ 0 & 0 & 0 & \bar{Q}_{PE24} & \bar{Q}_{PE25} & 0 & \bar{Q}_{DE22} & 0 \\ \bar{Q}_{PE31} & \bar{Q}_{PE32} & \bar{Q}_{PE36} & 0 & 0 & 0 & 0 & \bar{Q}_{DE33} \end{bmatrix} \times \begin{Bmatrix} (\varepsilon_{xx} - e_x) \\ (\varepsilon_{yy} - e_y) \\ (\gamma_{xy} - e_{xy}) \\ \gamma_{yz} \\ \gamma_{xz} \\ (E_x - \bar{E}_x) \\ (E_y - \bar{E}_y) \\ (E_z - \bar{E}_z) \end{Bmatrix}. \tag{12}$$

In the above equation, the transformed elastic part is well known. Therefore, only the piezoelectric, pyroelectric and hygro-thermo-elastic parts are given below:

$$\begin{aligned}
&e_x = e_1 m^2 + e_2 n^2, \quad e_y = e_1 n^2 + e_2 m^2, \quad e_{xy} = (e_1 - e_2)mn, \\
&\bar{E}_x = P_1 T, \quad \bar{E}_y = P_2 T, \quad \bar{E}_z = P_3 T, \\
&\bar{Q}_{PE31} = Q_{PE31} m^2 + Q_{PE32} n^2, \quad \bar{Q}_{PE32} = Q_{PE31} n^2 + Q_{PE32} m^2, \\
&\bar{Q}_{PE36} = (Q_{PE31} - Q_{PE32})mn, \quad \bar{Q}_{PE14} = (Q_{PE15} + Q_{PE24})mn, \\
&\bar{Q}_{PE25} = -(Q_{PE15} + Q_{PE24})mn, \quad \bar{Q}_{PE24} = Q_{PE24} m^2 - Q_{PE15} n^2, \\
&\bar{Q}_{PE15} = Q_{PE15} m^2 - Q_{PE24} n^2, \quad m = \cos\theta, \ \ n = \sin\theta, \\
&Q_{PE31} = d_{31} - \frac{C_{13} d_{33}}{C_{33}}; \quad Q_{PE32} = d_{32} - \frac{C_{23} d_{33}}{C_{33}}; \quad Q_{PE24} = d_{24}; \quad Q_{PE15} = d_{15}; \\
&Q_{DE11} = \kappa_{11}; \quad Q_{DE22} = \kappa_{22}; \quad Q_{DE33} = \kappa_{33} + \frac{d_{33} d_{33}}{C_{33}}; \\
&e_1 = \alpha_1 T + \beta_1 \chi; \quad e_2 = \alpha_2 T + \beta_2 \chi; \\
&\bar{E}_1 = P_1 T; \quad \bar{E}_2 = P_2 T; \quad \bar{E}_3 = P_3 T.
\end{aligned} \tag{13}$$

Note that subscripts PE and DE denote piezoelectric and dielectric, respectively.

4. FE formulation

A doubly curved shell element is shown in Fig. 1 with co-ordinates x, y along the in-plane direction and z along the thickness direction. The linear displacement relations are given by

$$u(x,y,z,t) = u_0(x,y,t) + z\theta_y(x,y,t),$$
$$v(x,y,z,t) = v_0(x,y,t) - z\theta_x(x,y,t),$$
$$w(x,y,z,t) = w(x,y,t), \tag{14}$$

where u_0, v_0,and w are the mid-plane displacements and θ_x and θ_y are the rotations of the cross-sections in the YZ and XZ planes, respectively.

Two multifunctional layers are considered in the formulation and they can be placed anywhere along the thickness direction of the laminate (kth layer, see Fig. 1). The active layers can be used either as actuators or as sensors in the distributed active control. The total electric potential in each active layer (subscript a denotes actuator and s denotes sensor) is given by

$$\phi_a(x,y,z) = \phi_{0a}(x,y) + \frac{(z-h_{k-1})}{(h_k-h_{k-1})}\phi_{1a}(x,y),$$
$$\phi_s(x,y,z) = \phi_{0s}(x,y) + \frac{(z-h_{k-1})}{(h_k-h_{k-1})}\phi_{1s}(x,y), \tag{15}$$

where ϕ_0 is the mean electric potential defined at the mid-plane of the active layer and ϕ_1 is the difference of potential between top and bottom surfaces of the active layer. It is assumed that the electric potential variation across the thickness is linear.

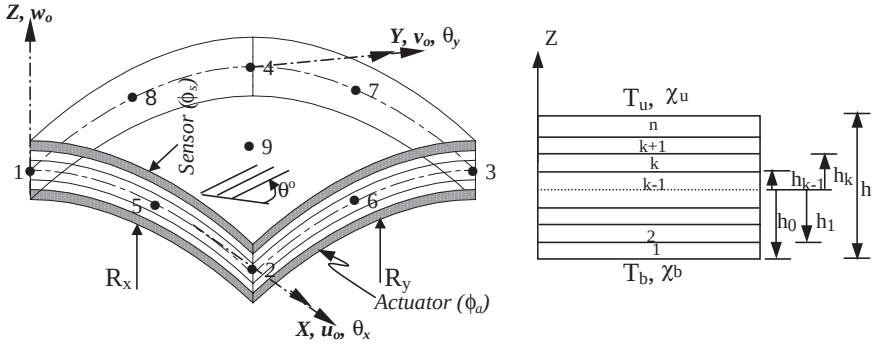

Fig. 1. Doubly curved laminated shell element with active layers.

The linear gradient relations are described for mechanical field as follows:

$$\{\varepsilon^l\} = \{\varepsilon_m\} + z\{\varepsilon_b\},$$

$$\{\varepsilon_m\} = \begin{Bmatrix} \varepsilon_x^m \\ \varepsilon_y^m \\ \gamma_{xy}^m \end{Bmatrix} = \begin{Bmatrix} \left(\dfrac{\partial u_o}{\partial x} + \dfrac{w}{R_x}\right) \\ \left(\dfrac{\partial v_o}{\partial y} + \dfrac{w}{R_y}\right) \\ \left(\dfrac{\partial u_o}{\partial y} + \dfrac{\partial v_o}{\partial x}\right) \end{Bmatrix},$$

$$\{\varepsilon_b\} = \begin{Bmatrix} \varepsilon_x^b \\ \varepsilon_y^b \\ \gamma_{xy}^b \end{Bmatrix} = \begin{Bmatrix} \left(\dfrac{\partial \theta_y}{\partial x}\right) \\ -\left(\dfrac{\partial \theta_x}{\partial y}\right) \\ \left(\dfrac{\partial \theta_y}{\partial y} - \dfrac{\partial \theta_x}{\partial x}\right) - C_2\left(\dfrac{1}{R_y} - \dfrac{1}{R_x}\right)\left(\dfrac{\partial v_o}{\partial x} - \dfrac{\partial u_o}{\partial y}\right) \end{Bmatrix},$$

$$\{\varepsilon_s\} = \begin{Bmatrix} \gamma_{xz} \\ \gamma_{yz} \end{Bmatrix} = \begin{Bmatrix} \left(\dfrac{\partial w}{\partial x} + \theta_y - C_1\dfrac{u_o}{R_x}\right) \\ \left(\dfrac{\partial w}{\partial y} - \theta_x - C_1\dfrac{v_o}{R_y}\right) \end{Bmatrix}, \tag{16}$$

where R_x and $R_{y,}$ are the two radii of curvature of the shell element and C_1 and C_2 are the shell theory tracers by which the analysis can be reduced to that of Sander's, Love's and Donnell's theories.

The linear gradient relations for the electric field are defined by

$$\{E\}_i = \{\, E_x \quad E_y \quad E_z \,\}^{\mathrm{T}},$$
$$= \left\{ -\frac{\partial \phi_i}{\partial x} \quad -\frac{\partial \phi_i}{\partial y} \quad -\frac{\partial \phi_i}{\partial z} \right\}^{\mathrm{T}}, \tag{17}$$

where $i = a, s$, a is the actuator and s is the sensor.

The elemental mechanical and electrical degrees of freedom fields are isoparametrically interpolated using linear shape functions (N_i):

$$\{u^e \phi^e\}^{\mathrm{T}} = \sum_{i=1,9} N_i \{\bar{u} \;\; \bar{\phi}\}_i^{\mathrm{T}}, \tag{18}$$

where $\{\bar{u}\} = \{u_0 \;\; v_0 \;\; w \;\; q_x \;\; q_y\}^{\mathrm{T}}$ and $\{\bar{\phi}\} = \{\phi_{1a} \;\; \phi_{1s}\}^{\mathrm{T}}$ are the nodal vectors of mechanical and electrical degrees of freedom, respectively.

Upon substituting Eqs. (14), (15) and (18) into gradient relations, we get

$$\{\varepsilon\} = \sum_{i=1,9} [J]^{-1}[B_u]_i \{\bar{u}\}_i \quad \text{and} \quad \{E\} = \sum_{i=1,9} [J]^{-1}[B_\phi]_i \{\bar{\phi}\}_i, \tag{19}$$

where $[J]$ is a Jacobian matrix and $[B_u]$ and $[B_\phi]$ are the shape function derivative matrices of the elastic and electric fields, respectively.

Using Eqs. (18) and (19), together with the material constitutive relations, the energy equation (11) is minimized for a stationary value to derive the governing FE equations in terms of nodal displacements and nodal voltages:

$$[M_{uu}]\{\ddot{\bar{u}}\} + [K_{uu}]\{\bar{u}\} - [K_G^e]\{\bar{u}\} + [K_{u\phi}]\{\bar{\phi}\} = \{F_m\} + \{F_{HT}\}, \tag{20}$$

$$[K_{\phi u}]\{\bar{u}\} + [K_{\phi\phi}]\{\bar{\phi}\} = \{F_{el}\} + \{F_{ET}\}, \tag{21}$$

where K_G^e is the geometric stiffness matrix due to induced stresses by temperature and moisture, F_m is the applied mechanical load, $\{F_{\mathrm{HT}}\}$ is the hygrothermal load vector and $\{F_{\mathrm{ET}}\}$ is the electrothermal load vector. In Eq. (21), the applied charge $\{F_{el}\}$ is zero for sensor application.

And the element matrices are calculated as follows:

$$[M_{uu}] = \int\int [N_u]^{\mathrm{T}}[\bar{\rho}][N_u]|J|\,\mathrm{d}\xi\,\mathrm{d}\eta; \quad [K_{uu}] = \int\int [B_u]^{\mathrm{T}}[\bar{c}][B_u]|J|\,\mathrm{d}\xi\,\mathrm{d}\eta;$$

$$[K_{u\phi}] = \int\int [B_u]^{\mathrm{T}}[\bar{d}][B_\phi]|J|\,\mathrm{d}\xi\,\mathrm{d}\eta; \quad [K_{\phi\phi}] = \int\int [B_\phi]^{\mathrm{T}}[\bar{\kappa}][B_\phi]|J|\,\mathrm{d}\xi\,d\eta;$$

$$[K_{\phi u}] = [K_{u\phi}]^{\mathrm{T}}; \quad \{F_{el}\} = \frac{\kappa_{33}}{(h_k - h_{k-1})} \int\int [N_\phi]^{\mathrm{T}}\phi|J|\,\mathrm{d}\xi\,\mathrm{d}\eta.$$

The integration is carried out with limits -1 to $+1$. The material constitutive matrices are given by

$$[\bar{c}] = \begin{bmatrix} [A] & [B] & 0 \\ [B] & [D] & 0 \\ 0 & 0 & [A^s] \end{bmatrix}, \quad [\bar{d}] = \begin{bmatrix} [A_{PE}] & 0 \\ [B_{PE}] & 0 \\ [A^s_{PE}] & [B^s_{PE}] \end{bmatrix}, \quad [\bar{\kappa}] = \begin{bmatrix} [A_{DE}] & 0 \\ 0 & [D_{DE}] \end{bmatrix}, \tag{22}$$

where

$$(A_{ij}, B_{ij}, D_{ij}) = \sum_{k=1}^{n} \int_{z_{k-1}}^{z_k} (\bar{Q}_{ij})_k (1, z, z^2)\,\mathrm{d}z \quad (i,j = 1,2,6),$$

$$(A^s_{ij}) = SCF \sum_{k=1}^{n} \int_{z_{k-1}}^{z_k} (\bar{Q}_{ij})_k\,\mathrm{d}z \quad (i,j = 4,5),$$

$$(A_{PEij}, B_{PEij}) = \sum_{k=1}^{n} \int_{z_{k-1}}^{z_k} (\bar{Q}_{PEij})_k (1, z)\,\mathrm{d}z \quad (i = 3;\ j = 1,2,6),$$

$$(A^s_{PEij}, B^s_{PEij}) = \sum_{k=1}^{n} \int_{z_{k-1}}^{z_k} (\bar{Q}_{PEij})_k (1, z)\,\mathrm{d}z \ \ (i = 1,2;\ j = 4,5),$$

$$(A_{DE}, D_{DE}) = \sum_{k=1}^{n} \int_{z_{k-1}}^{z_k} (\bar{Q}_{DEij})_k (1, z^2)\,\mathrm{d}z \ \ (i,j = 1,2,3).$$

The shear correction factor (SCF) is taken as 5/6 in the present analysis. The $[\bar{\rho}]$ is the mass property matrix and is defined by

$$[\bar{\rho}] = \begin{bmatrix} I_n & 0 & 0 & 0 & 0 \\ 0 & I_n & 0 & 0 & 0 \\ 0 & 0 & I_n & 0 & 0 \\ 0 & 0 & 0 & I_r & 0 \\ 0 & 0 & 0 & 0 & I_r \end{bmatrix}, \quad (I_n, I_r) = \sum_{k=1}^{n} \int_{z_{k-1}}^{z_k} \rho_k(1, z^2)\, \mathrm{d}z. \tag{23}$$

4.1. Hygrothermal load vector and element initial stress stiffness matrix

The element load vector due to hygro-thermo-elastic forces and moments is given by

$$F_{HT} = \int\int [B_u]^{\mathrm{T}} \{F_N\} |J|\, \mathrm{d}\xi\, \mathrm{d}\eta, \tag{24}$$

where $\{F_N\} = \{\, N_x^e \quad N_y^e \quad N_{xy}^e \quad M_x^e \quad M_y^e \quad M_{xy}^e \quad 0 \quad 0\}^{\mathrm{T}}$, superscript e stands for hygrothermal strain. The thermoelastic forces and moments can be expressed as

$$\left\{ \{N^{\mathrm{T}}\} \quad \{M^{\mathrm{T}}\} \right\} = \sum_{k=1}^{n} \int_{z_{k-1}}^{z_k} \{\bar{\lambda}\}\, T(1,\ z)\, \mathrm{d}z,$$

where

$$T = T_0 + \frac{z}{h} T_1 \quad \text{with } T_0 = \frac{(T_u + T_b)}{2},\ T_1 = (T_u - T_b) \tag{25}$$

and T_0 and T_1 are the mean and difference of temperatures, respectively. The hygroelastic forces and moments can be expressed as

$$\left\{ \{N^{\chi}\} \quad \{M^{\chi}\} \right\} = \sum_{k=1}^{n} \int_{z_{k-1}}^{z_k} \{\bar{\Lambda}\} \chi(1, z)\, \mathrm{d}z,$$

where

$$\chi = \chi_0 + \frac{z}{h} \chi_1 \quad \text{with } \chi_0 = \frac{(\chi_u + \chi_b)}{2},\ \chi_1 = (\chi_u - \chi_b) \tag{26}$$

and χ_0 and χ_1, are the mean and difference of moisture concentrations, respectively. It may be noted that $\bar{\lambda}$ and $\bar{\Lambda}$ are the transformed thermo- and hygroelastic constants, respectively. The non-linear strains of the doubly curved element are expressed, following Lee and Yen [15], as

$$\{\varepsilon^{nl}\} = \begin{Bmatrix} \varepsilon_{xx}^{nl} \\ \varepsilon_{yy}^{nl} \\ \gamma_{xy}^{nl} \\ \gamma_{xz}^{nl} \\ \gamma_{yz}^{nl} \end{Bmatrix} = \begin{Bmatrix} \frac{1}{2}\left[(u_{,x} + w/R_x)^2 + (v_{,x})^2 + (w_{,x} - u/R_x)^2\right] \\ \frac{1}{2}\left[(u_{,y})^2 + (v_{,y} + w/R_y)^2 + (w_{,y} - v/R_y)^2\right] \\ \left[u_{,y}(u_{,x} + w/R_x) + v_{,x}(v_{,y} + w/R_y) + (w_{,x} - u/R_x)(w_{,y} - v/R_y)\right] \\ \left[u_{,z}(u_{,x} + w/R_x) + v_{,x}v_{,z} + w_{,z}(w_{,x} - u/R_x\right] \\ \left[u_{,y}u_{,z} + v_{,z}(v_{,y} + w/R_y) + w_{,z}(w_{,y} - v/R_y)\right] \end{Bmatrix}, \tag{27}$$

where w is assumed to be constant across the thickness (z direction). The non-linear strains in Eq. (27) are expressed in matrix form as

$$\left\{ \varepsilon_{xx}^{nl} \quad \varepsilon_{yy}^{nl} \quad \gamma_{xy}^{nl} \quad \gamma_{xz}^{nl} \quad \gamma_{yz}^{nl} \right\}^{\mathrm{T}} = \tfrac{1}{2}[\bar{R}]\{\delta_e\}, \tag{28}$$

where $\{\delta_e\} = \{u_{o,x}, u_{o,y}, v_{o,x}, v_{o,y}, w_{,x}, w_{,y}, \theta_{x,x}, \theta_{x,y}, \theta_{y,x}, \theta_{y,y}, \theta_x, \theta_y, u_o, v_o, w\}^{\mathrm{T}}$ and matrix $\bar{R}$ can be obtained from Eqs. (27) and (28).

Using Eq. (18), $\{\delta_e\}$ may be expressed as

$$\{\delta_e\}_i = \sum_{i=1,9} [G]_i \{\bar{u}\}_i, \tag{29}$$

where

$$[G]_i = \begin{Bmatrix} N_{i,x} & 0 & 0 & 0 & 0 \\ N_{i,y} & 0 & 0 & 0 & 0 \\ 0 & N_{i,x} & 0 & 0 & 0 \\ 0 & N_{i,y} & 0 & 0 & 0 \\ 0 & 0 & N_{i,x} & 0 & 0 \\ 0 & 0 & N_{i,y} & 0 & 0 \\ 0 & 0 & 0 & N_{i,x} & 0 \\ 0 & 0 & 0 & N_{i,y} & 0 \\ 0 & 0 & 0 & 0 & N_{i,x} \\ 0 & 0 & 0 & 0 & N_{i,y} \\ 0 & 0 & 0 & N_i & 0 \\ 0 & 0 & 0 & 0 & N_i \\ N_i & 0 & 0 & 0 & 0 \\ 0 & N_i & 0 & 0 & 0 \\ 0 & 0 & N_i & 0 & 0 \end{Bmatrix}.$$

The potential energy due to induced stresses by temperature and moisture can be expressed as

$$U_{PE}^e = \tfrac{1}{2} \int \{\delta_e\}^{\mathrm{T}} [G]^{\mathrm{T}} [\bar{R}]^{\mathrm{T}} \{\sigma^e\} \, \mathrm{d}v,$$

$$[\bar{R}]^{\mathrm{T}} \{\sigma^e\} = \{\sigma^e\}[G]\{\delta_e\}, \tag{30}$$

where $\{\sigma^e\}$ is arranged in matrix form as follows:

$$
[\sigma^e] = \begin{bmatrix}
\sigma_x^e & & & & & & & & & & & & & & \\
\sigma_{xy}^e & \sigma_y^e & & & & & & & & & & & & & \\
0 & 0 & \sigma_x^e & & & & & & & & & & & & \\
0 & 0 & \sigma_{xy}^e & \sigma_y^e & & & & & & & & & & & \\
0 & 0 & 0 & 0 & \sigma_x^e & & & & & & & & & & \\
0 & 0 & 0 & 0 & \sigma_{xy}^e & \sigma_y^e & & & & & & & & & \\
0 & 0 & -z\sigma_x^e & -z\sigma_{xy}^e & 0 & 0 & z^2\sigma_x^e & & & & & & & & \\
0 & 0 & -z\sigma_{xy}^e & -z\sigma_y^e & 0 & 0 & z^2\sigma_{xy}^e & z^2\sigma_y^e & & & & & & & \\
z\sigma_x^e & z\sigma_{xy}^e & 0 & 0 & 0 & 0 & 0 & 0 & z^2\sigma_x^e & & & & & & \\
z\sigma_{xy}^e & z\sigma_y^e & 0 & 0 & 0 & 0 & 0 & 0 & z^2\sigma_{xy}^e & z^2\sigma_y^e & & & & & \\
0 & 0 & \tau_{xz}^e & -\tau_{yz}^e & z\sigma_{xy}^e & z\sigma_y^e & -z\tau_{xz}^e & z\tau_{yz}^e & 0 & 0 & \dfrac{z^2\sigma_y^e}{R_y^2} & & & & \\
\tau_{xz}^e & \tau_{yz}^e & 0 & 0 & -z\sigma_x^e & -z\sigma_{xy}^e & 0 & 0 & z\tau_{xz}^e & z\tau_{yz}^e & \dfrac{z^2\sigma_{xy}^e}{R_xR_y} & \dfrac{z^2\sigma_x^e}{R_x^2} & & & \\
0 & 0 & 0 & 0 & -\dfrac{\sigma_x^e}{R_x} & -\dfrac{\sigma_{xy}^e}{R_x} & 0 & 0 & 0 & 0 & \dfrac{-z\sigma_{xy}^e}{R_xR_y} & \dfrac{z\sigma_x^e}{R_x^2} & \dfrac{\sigma_x^e}{R_x^2} & & \\
0 & 0 & 0 & 0 & -\dfrac{\sigma_y^e}{R_y} & -\dfrac{\sigma_y^e}{R_y} & 0 & 0 & 0 & 0 & \dfrac{-z\sigma_y^e}{R_y^2} & \dfrac{z\sigma_{xy}^e}{R_xR_y} & \dfrac{\sigma_{xy}^e}{R_xR_y} & \dfrac{\sigma_y^e}{R_y^2} & \\
\dfrac{\sigma_x^e}{R_x} & \dfrac{\sigma_{xy}^e}{R_x} & \dfrac{\sigma_{xy}^e}{R_y} & \dfrac{\sigma_y^e}{R_y} & 0 & 0 & \dfrac{-z\sigma_{xy}^e}{R_y} & \dfrac{-z\sigma_y^e}{R_y} & \dfrac{z\sigma_x^e}{R_x} & \dfrac{z\sigma_{xy}^e}{R_x} & \dfrac{-\tau_{yz}^e}{R_y} & \dfrac{\tau_{xz}^e}{R_x} & 0 & 0 & \dfrac{\sigma_x^e}{R_x^2}+\dfrac{\sigma_y^e}{R_y^2}
\end{bmatrix}
$$

Eq. (30) may be modified as

$$U_{PE}^e = \frac{1}{2}\int \{\delta_e\}^{\mathrm{T}}[G]^{\mathrm{T}}[\sigma^e][G]\{\delta_e\}\,\mathrm{d}v = \tfrac{1}{2}\{\delta_e\}^{\mathrm{T}}[K_G^e]\{\delta_e\}, \tag{31}$$

where $[K_G^e] = \int [G]^{\mathrm{T}}[S^e][G]|J|\,\mathrm{d}\xi\,\mathrm{d}\eta$. The geometric stiffness matrix $[K_G^e]$ can be expressed in terms of stress resultants due to temperature and moisture as

$$[K_G^e] = \int_{-1}^{1}\int_{-1}^{1} [G]^{\mathrm{T}}[S^e][G]|J|\,\mathrm{d}\xi\,\mathrm{d}\eta. \tag{32}$$

The matrix $[S^e]$ is defined by

$$[S^e] = \begin{bmatrix}
N_x^e & & & & & & & & & & & & & & \\
N_{xy}^e & N_y^e & & & & & & & & & & & & & \\
0 & 0 & N_x^e & & & & & & & & & & & & \\
0 & 0 & N_{xy}^e & N_y^e & & & & & & & & & & & \\
0 & 0 & 0 & 0 & N_x^e & & & & & & & & & & \\
0 & 0 & 0 & 0 & N_{xy}^e & N_y^e & & & & & & & & & \\
0 & 0 & -M_x^e & -M_{xy}^e & 0 & 0 & \frac{N_x^e h^2}{12} & & & & & & & & \\
0 & 0 & -M_{xy}^e & -M_y^e & 0 & 0 & \frac{N_{xy}^e h^2}{12} & \frac{N_y^e h^2}{12} & & & & & & & \\
M_x^e & M_{xy}^e & 0 & 0 & 0 & 0 & 0 & 0 & \frac{N_x^e h^2}{12} & & & & & & \\
M_{xy}^e & M_y^e & 0 & 0 & 0 & 0 & 0 & 0 & \frac{N_{xy}^e h^2}{12} & \frac{N_y^e h^2}{12} & & & & & \\
0 & 0 & Q_x^e & -Q_y^e & M_{xy}^e & M_y^e & -hQ_x^e & hQ_y^e & 0 & 0 & \frac{N_y^e h^2}{12R_y^2} & & & & \\
Q_x^e & Q_y^e & 0 & 0 & -M_x^e & -M_{xy}^e & 0 & 0 & hQ_x^e & hQ_y^e & \frac{N_{xy}^e h^2}{12R_xR_y} & \frac{N_x^e h^2}{12R_x^2} & & & \\
0 & 0 & 0 & 0 & -\frac{N_x^e}{R_x} & -\frac{N_{xy}^e}{R_x} & 0 & 0 & 0 & 0 & \frac{-M_{xy}^e}{R_xR_y} & \frac{M_x^e}{R_x^2} & \frac{N_x^e}{R_x^2} & & \\
0 & 0 & 0 & 0 & -\frac{N_{xy}^e}{R_y} & -\frac{N_y^e}{R_y} & 0 & 0 & 0 & 0 & \frac{-M_y^e}{R_y^2} & \frac{M_{xy}^e}{R_xR_y} & \frac{N_{xy}^e h^2}{12R_xR_y} & \frac{N_y^e}{R_y^2} & \\
\frac{N_x^e}{R_x} & \frac{N_{xy}^e}{R_x} & \frac{N_{xy}^e}{R_y} & \frac{N_y^e}{R_y} & 0 & 0 & \frac{-M_{xy}^e}{R_y} & \frac{-M_y^e}{R_y} & \frac{M_x^e}{R_x} & \frac{M_{xy}^e}{R_x} & \frac{-Q_y^e}{R_y} & \frac{Q_x^e}{R_x} & 0 & 0 & \frac{N_x^e}{R_x^2}+\frac{N_y^e}{R_y^2}
\end{bmatrix} \tag{33}$$

The matrix $[S]$ is evaluated using the stress resultants (N^e, M^e) due to hygrothermal loads (Eqs. (24)–(26)). The geometric stiffness matrix $[K_G^e]$ is obtained with the 3×3 Gauss quadrature.

4.2. Solution process

The global dynamic equation with feedback force is given by

$$[M_{uu}]\{\ddot{\bar{u}}\} + [K_{uu}]\{\bar{u}\} - [K_G^e]\{\bar{u}\} = \{F_m\} + \{F_{HT}\} - \{F_{feed}\}, \tag{34}$$

where $\{F_{feed}\} = [K_{u\phi}]\{\phi_a\}$, $\phi_a$is the actuator voltage.

The dynamic analysis of piezo-hygro-thermo-elastic laminate is carried out, solving the following equation:

$$([K_{uu}] - [K_G^e] + [K_a] - \lambda[M_{uu}])\{\bar{u}\} = 0. \tag{35}$$

The active stiffness matrix $[K_a]$ is formulated in the FE analysis, employing the coupled piezoelectric matrices ($K_{u\phi}$, $K_{\phi\phi}$) as follows:

$$[K_a] = [K_{u\phi}][F_d][K_{\phi\phi}]^{-1}[K_{\phi u}], \tag{36}$$

where F_d is the displacement control gain and a unit gain is assumed in the present analysis.

The stress stiffening effect due to piezoelectric actuation is included in the present analysis using the actuator and sensor matrices to study the influence of active stiffening on the closed loop system frequencies. However, the actuation effect may also be considered through the geometric stiffness matrix, derived from piezoelectric stress resultants by applying specified actuator voltage in the uncoupled analysis.

5. Numerical studies

5.1. Validation problems

The developed FE procedures are coded in MATLAB® and the element is thoroughly validated for its performance to solve the dynamic problems of laminated plates/shells with stress stiffening and piezoelectric effects. The element is made field consistent by adopting a selective integration technique (3×3 for membrane and bending; 3×2, 2×3 for shear).

5.1.1. Free vibration analysis

The symmetric and un-symmetric simply supported laminated cylindrical ($R_x = R$) and spherical ($R_x = R_y = R$) shells are considered with different a/h and R/a ratios. The following material properties are used in the analysis:

$$E_1 = 25E_2, \quad G_{23} = 0.2E_2, \quad G_{13} = G_{12} = 0.5E_2, \quad v_{12} = 0.25.$$

The free vibration frequencies of laminated plates and shells are presented in Tables 1 and 2. The predicted natural frequencies by the present element are in good agreement with those reported by Reddy [16]. The close correlation shows the capability of present element to model the dynamics of thin and moderately thick composite plates and shells. As another validation problem for the dynamics of moderately thick laminates, simply supported cross-ply laminated plate ($a/h = 10$) is considered. The analysis is carried out, taking the material data as given in Ref. [13]. The free vibration frequencies estimated by the present element (FSDT) are compared

Table 1
Non-dimensional fundamental frequency ($\bar{\omega} = \omega a^2\sqrt{\rho/E_2}/h$) versus radius to side length ratio of spherical shell ($a/b = 1$)

R/a	0°/90°				0°/90°/0°				0°/90°/90°/0°			
	$a/h = 100$		$a/h = 10$		$a/h = 100$		$a/h = 10$		$a/h = 100$		$a/h = 10$	
	$\bar{\omega}$	$\bar{\omega}^*$	$\bar{\omega}$	$\bar{\omega}^*$	$\bar{\omega}$	$\bar{\omega}^*$	$\bar{\omega}$	$\bar{\omega}^*$	$\bar{\omega}$	$\bar{\omega}^*$	$\bar{\omega}$	$\bar{\omega}^*$
1	125.956	125.930	14.454	14.481	126.016	125.990	16.087	16.115	126.349	126.330	16.148	16.172
2	67.376	67.361	10.744	10.749	68.088	68.075	13.376	13.382	68.307	68.294	13.441	13.447
3	46.011	46.002	9.781	9.761	47.274	47.265	12.729	12.731	47.424	47.415	12.794	12.795
4	35.235	35.228	9.410	9.410	36.978	36.971	12.487	12.487	37.089	37.082	12.552	12.552
5	28.831	28.825	9.231	9.231	30.999	30.993	12.372	12.372	31.084	31.079	12.437	12.437
10	16.708	16.706	8.985	8.984	20.349	20.347	12.216	12.215	20.383	20.380	12.281	12.280
10E30	9.688	9.687	8.900	8.900	15.184	15.183	12.163	12.162	15.185	15.184	12.228	12.226

$\bar{\omega}^*$—Ref. [16]; $\bar{\omega}$—present element.

with those results predicted by other theories (TSDPT, LWPT, PLWPT, CLPT) and exact solution (refer Table 3). A close correlation of results shows that the present element may be used to analyze the moderately thick laminates.

5.1.2. Thermoelastic and hygroelastic validation

Since the stress stiffening effect by hygrothermal strain is introduced in the FE formulation, a thorough analysis is carried out to qualify the present element. Firstly a thermal buckling problem is solved for both isotropic and piezolaminated composite plates. The dimension, material data and boundary conditions are taken as defined in Refs. [12,13]. The buckling temperatures predicted by the present element are presented along with those reported results [12,13] in Tables 4(a) and (b) and 5. A good comparison is observed for the buckling temperature and the analysis reveals that the geometric stiffness matrix is correctly modelled in the present FE formulation. Next, a validation problem for piezo-thermo-elastic coupling is presented. The piezolaminated plate dimension and material data are considered as given in Ref. [7]. The applied uniform

Table 2
Non-dimensional fundamental frequency ($\bar{\omega} = \omega a^2\sqrt{\rho/E_2}/h$) versus radius to side length ratio of cylindrical shell ($a/b = 1$)

R/a	0°/90°				0°/90°/0°				0°/90°/90°/0°			
	$a/h = 100$		$a/h = 10$		$a/h = 100$		$a/h = 10$		$a/h = 100$		$a/h = 10$	
	$\bar{\omega}$	$\bar{\omega}^*$	$\bar{\omega}$	$\bar{\omega}^*$	$\bar{\omega}$	$\bar{\omega}^*$	$\bar{\omega}$	$\bar{\omega}^*$	$\bar{\omega}$	$\bar{\omega}^*$	$\bar{\omega}$	$\bar{\omega}^*$
1	65.508	65.474	10.038	9.999	66.608	66.583	13.187	13.172	66.737	66.704	13.145	13.128
2	34.932	34.914	9.164	9.148	36.782	36.770	12.443	12.438	36.874	36.858	12.477	12.471
3	24.528	24.516	8.993	8.983	27.123	27.116	12.290	12.287	27.183	27.173	12.340	12.337
4	19.518	19.509	8.937	8.930	22.714	22.709	12.235	12.233	22.756	22.749	12.291	12.289
5	16.674	16.668	8.913	8.909	20.337	20.332	12.209	12.207	20.367	20.361	12.269	12.267
10	11.834	11.831	8.891	8.888	16.626	16.625	12.175	12.173	16.636	16.634	12.238	12.236
10E30	9.688	9.687	8.901	8.900	15.184	15.183	12.163	12.162	15.185	15.184	12.228	12.226

$\bar{\omega}^*$—Ref. [16]; $\bar{\omega}$—present element.

Table 3
Comparison of non-dimensional natural frequencies for simply supported [0/90/0] laminated square plate ($a/h = 10$: $\varpi = \omega h\sqrt{(\rho/E_2)}$)

Theory	ϖ_1	ϖ_2	ϖ_3	ϖ_4
Nosier et al. [21] (Exact)	0.06715	0.12811	0.17217	0.20798
Nosier et al. [21] (TSDPT)	0.06839	0.13010	0.17921	0.21526
Nosier et al. [21] (FSDPT)	0.06931	0.12886	0.18674	0.22055
Nosier et al. [21] (CLPT)	0.07769	0.15185	0.26599	0.31077
Carrera [20] (LWPT)	0.06758	—	—	0.21100
Present 9 node element[a] (FSDT)	0.06839	0.12832	0.18775	0.22069
Oh et al. [13] (PLWPT)	0.06629	0.12862	0.17364	0.20913

[a] Selective integration.

Table 4
Verification of critical buckling temperature for isotropic square plates ($a/h = 100$, $\alpha = 2 \times 10^{-6}$, $v = 0.3$)

Sl no	Temperature distribution	Present FE	Analytical	Thangaratnam et al. [22]	Oh et al. [12]
		(a) *Simply supported (S–S–S–S)*			
1	Uniform temperature rise	63.215	63.27	63.33	62.51
2	Linearly varying temperature in x direction	126.43	126.54	126.00	—
3	Linearly varying temperature in x and y directions.	252.86	252.00	250.65	—
		(b) *Clamped (C–C–C–C)*			
1	Uniform temperature rise	169.09	168.71	167.70	167.72
2	Linearly varying temperature in x direction	338.19	337.42	332.50	—
3	Linearly varying temperature in x and y directions	667.47	674.84	657.84	—

Table 5
Comparison of Euler buckling temperature of simply supported piezolaminated composite plates ($a/h = 100$)

Theory	Euler buckling temperature (°C)
Present element	50.590
Oh et al. [13] (SF)	50.241
Present element	52.075
Oh et al. [13] (EF)	52.632

temperature develops the electric potential due to the presence of direct piezoelectric coupling. The thermally induced sensory deflection pattern is plotted along with those results of Lee and Saravanos [7] in Fig. 2. The transverse deflections predicted by the present element are seen closely correlating with the shell element results of Lee and Saravanos [7].

A simply supported laminated plate (CFRP) subjected to uniform temperature and moisture is considered as another validation problem for stress stiffening effect. The material data considered for the analysis are given in Table 6. The estimated free vibration frequencies are presented in Table 7 along with Ritz solutions [19]. The dynamic analysis results reflect that the stress stiffening effect due to expansion strain is correctly captured by the present element.

5.1.3. Piezoelectric validation

The coupled piezoelectric matrices will be used in the active stiffness estimation; thus, a validation problem for piezoelectric coupling is presented. A simply supported, laminated plate

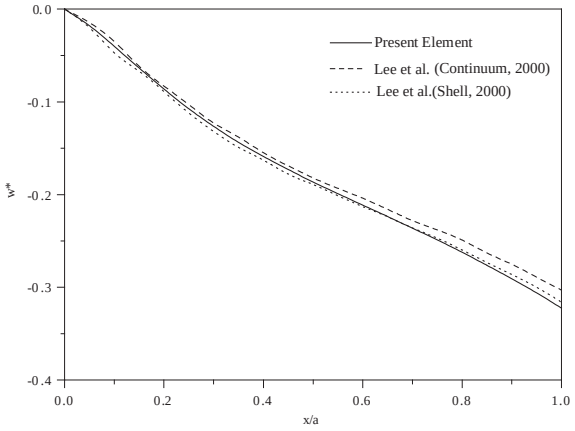

Fig. 2. Verification of thermally induced sensory displacement of a clamped piezolaminated plate (0_8/PZT).

Table 6
Material data used in the present analysis

Material properties	CFRP	PZT	CFRP*	PVDF
Elastic moduli (GPa)				
E_1	130	63.0	172.37	2.0
E_2, E_3	9.5	63.0	6.9	2.0
G_{12}, G_{13}	6.0	24.6	3.45	0.775
G_{23}	3.0	24.6	1.38	0.775
v_{12}, v_{13}, v_{23}	0.3	0.28	0.25	0.29
Coeff. of thermal expansion (/K)				
α_1	−0.3E−6	0.9E−6	—	—
α_2	28.1E−6	0.9E−6	—	—
Coeff. of moisture co-efficient (/%χ)				
β_1	0.0	—	—	—
β_2	0.44	—	—	—
Piezoelectric constant (C/N)				
d_{31}, d_{32}	—	250E−12	0.0	23E−12
Dielectric constant (F/m)				
κ_{11}, κ_{22}	—	15.3E–9	0.0	10.62E−9
κ_{33}	—	15.0E−9	0.0	10.62E−9
Density (kg/m^3)				
ρ	1600	7600	—	—

(CFRP*) is considered with PVDF layers at top and bottom. The material properties used in the analysis are presented in Table 6. The piezoelectrically induced displacements and stresses are estimated (see Table 8) and are found to be in good comparison with exact and FE results [17,18].

Table 7
Verification of non-dimensionalized natural frequencies in comparison with Ritz method ($a/b = 1$, $a/h = 100$, [0°/90°/90°/0°])

Mode no.	Elastic, $\chi_0 = 0\%$, $T_0 = 0\,K$	$\chi_0 = 0.1\%$			$T_0 = 325\,K$		
		Present	Ritz method	Eight-noded element [19]	Present	Ritz Method	Eight-noded element [19]
1	12.0432	9.392	9.411	9.429	8.044	8.068	8.088
2	23.1842	19.881	19.911	20.679	18.342	18.378	19.196
3	41.1674	39.334	39.528	40.679	38.578	38.778	39.324
4	48.0229	45.593	45.815	46.752	44.546	44.778	45.431

Table 8
Verification of non-dimensional deflections and stresses of laminated simply supported square plate ([PVDF/0°/90°/0°/PVDF]; $a/h = 100$, applied load = 10 N/m^2)

	Applied voltage $\varphi_a = 0$				Applied voltage $\varphi_a = 100$			
	$\bar{u}$	$\bar{w}$	$\bar{\sigma}_{xx}$	$\bar{\sigma}_{yy}$	$\bar{u}$	$\bar{w}$	$\bar{\sigma}_{xx}$	$\bar{\sigma}_{yy}$
Present	∓0.0068	0.4421	±0.5524	±0.1859	∓0.00645	0.4202	+0.5174	0.1700
							−0.5227	−0.1801
Ref. [17]	∓0.0068	0.4450	±0.5590	±0.1870	∓0.0065	0.4209	+0.4980	0.1640
							−0.5240	−0.1910
Ref. [18]	∓0.0067	0.4710	±0.5380	±0.1810	−0.0063	0.4470	+0.5040	0.1580
					0.0065		−0.5180	−0.1840

The results of the validation problems show that the present element is capable of modelling the dynamic behaviour of piezo-hygro-thermo-elastic laminates.

5.2. Dynamic behaviour of piezo-hygro-thermo-elastic laminates

The piezoelectric lamina (PZT) can be effectively employed as a distributed actuator or sensor in feedback control application. As an actuator, it controls the amplitude of vibration and frequency through active effects, namely 'active stiffening' and 'active damping'. The active stiffening issue is attempted in the present paper. The angle-ply (45/−45) and cross-ply (0/90) laminates (CFRP: $a = 0.1\,m$, $b = 0.1\,m$) are taken for the numerical experiments with an additional active lamina (PZT: 0°, $h_{PZT} = 0.0002\,m$) as an actuator. Simply supported and clamped boundary conditions are assumed and the material data for the analysis is given in Table 6. The active stiffness is estimated using the coupled electromechanical stiffness ($K_{u\phi}$) and capacitance ($K_{\phi\phi}$) matrices, taking unit displacement gain. Hygral ($\chi_0 = 0.5\%$) and thermal ($T_0 = 350\,°K$) effects are introduced through initial stress stiffness matrix in the dynamic analysis. Thin ($a/h = 100$) and moderately thick ($a/h = 10$) piezo-hygro-thermo-elastic laminates (plates

and shells) are analyzed (mesh size 8×8) and the results are presented in the form of non-dimensional frequencies for various elastic modes with their respective mode order.

The boundary conditions adopted in the present analysis are:

Mechanical: $x = 0, a$; $v_0 = 0$, $w = 0$, $\theta_x = 0$ and $y = 0, b$; $u_0 = 0$, $w = 0$, $\theta_y = 0$.

Electrical: Short-circuit (electric potential = 0) and open-circuit (electric potential $\neq 0$).

5.2.1. Active stiffening and active compensation effects on plates

A parametric study is carried out to capture the active stiffening and active compensation effects on the dynamics of cross-ply and angle-ply laminated plates. The non-dimensional frequencies of different elastic modes are presented in Tables 9–12 for plates with $a/h = 10, 100$. In general, the frequency reduction in thin plates due to hygrothermal strain is relatively more for the clamped plates compared to simply supported plates. Also, the frequencies of thin piezoelectric clamped plates are enhanced substantially than simply supported plates due to active stiffening effect. It is noted that the active compensation to thermal effect is around ($\bar{\Omega}_{pte} \approx 6\%$) for clamped plates to ($\bar{\Omega}_{pte} \approx 5\%$) to simply supported plates. Similarly, the effect of hygral is also actively compensated by the piezoelectric actuation in clamped plates ($\bar{\Omega}_{phe} \approx 7\%$) as well as in simply supported plates ($\overline{\Omega}_{phe} \approx 5\%$). The hygral and thermal influence on frequency reduction of laminated plates with $a/h = 10$, is observed to be relatively less. Also, it is noted that the boundary effect on active stiffening is not very significant. The active stiffness introduced by piezoelectric coupling compensates the frequency reduction that has occurred due to hygrothermal effect in the case of moderately thick laminates ($a/h = 10$; Tables 11 and 12).

5.2.2. Active stiffening and active compensation effects on cylindrical shells

The cylindrical cross-ply and angle-ply laminated shells with $R_x/a = 10, 5$ are taken to study the stiffening effect on the frequency control and the results are presented in Tables 13–20. The reduction in elastic frequencies due to hygral and thermal effects is comparatively more in the case of clamped shells. Also the frequency reduction due to hygrothermal strain is relatively higher in the case of $R_x/a = 10$, compared to $R_x/a = 5$, for both cross-ply and angle-ply laminated shells. It is observed that the active stiffening is marginally influenced by boundary effect in thin shells

Table 9
Non-dimensional frequencies of piezo-hygro-thermo-elastic plates ($a/b = 1$, $a/h = 100$, S–S–S–S, $R/a = \infty$)

Laminate	Mode order	Ω_e	Ω_{te}	Ω_{he}	Ω_{pe}	Ω_{pte}	Ω_{phe}
0/90/PZT	1–1	9.1284	8.4688	8.1821	9.6193	8.8972	8.6513
	1–2	19.9740	19.1813	18.8379	20.8783	20.0490	19.7668
	2–1	26.8189	26.2035	25.9297	28.4468	27.7533	27.4996
	2–2	36.4658	35.5165	35.0608	38.4203	37.4276	37.0156
	1–3	38.9129	38.1180	37.7787	40.5667	39.7381	39.4630
45/−45/PZT	1–1	10.4514	8.7806	7.5274	10.9503	9.2513	8.0679
	1–2	22.2106	20.3507	19.0348	23.2671	21.3506	20.0879
	2–1	25.4945	23.9278	22.9540	26.9018	25.3325	24.4145
	1–3	37.8852	35.9489	34.6158	39.6976	37.6992	36.4065
	2–2	46.3335	44.9937	44.1492	48.7129	47.3187	46.5111

Table 10
Non-dimensional frequencies of piezo-hygro-thermo-elastic plates ($a/b = 1$, $a/h = 100$, C–C–C–C, $R/a = \infty$)

Laminate	Mode order	Ω_e	Ω_{te}	Ω_{he}	Ω_{pe}	Ω_{pte}	Ω_{phe}
0/90/PZT	1–1	17.7429	14.5812	12.3842	18.7901	15.8412	13.8515
	1–2	30.8129	26.5959	23.8389	32.2872	28.2917	25.7197
	2–1	41.0721	38.0265	36.1688	43.7366	40.8902	39.1695
	2–2	51.6875	47.8886	45.658	54.572	50.9884	48.3509
	1–3	53.0355	48.4682	45.5744	55.3714	51.0132	48.822
45/−45/PZT	1–1	17.1875	13.8642	11.4923	18.1476	15.0351	12.8838
	1–2	32.7699	28.7444	26.1458	34.4314	30.6178	28.1901
	2–1	36.6901	33.2581	31.1202	38.8194	35.5907	33.6009
	1–3	50.3398	46.2235	43.6891	52.9266	49.0094	46.6165
	2–2	61.3571	57.3811	54.9778	64.5861	60.815	58.5494

Table 11
Non-dimensional frequencies of piezo-hygro-thermo-elastic plates ($a/b = 1$, $a/h = 10$, S–S–S–S, $R/a = \infty$)

Laminate	Mode order	Ω_e	Ω_{te}	Ω_{he}	Ω_{pe}	Ω_{pte}	Ω_{phe}
0/90/PZT	1–1	8.4018	8.3901	8.3817	8.5411	8.5289	8.5202
	1–2	19.8782	19.8638	19.8535	20.0395	20.0248	20.0143
	2–1	20.9143	20.9007	20.8909	21.2986	21.2844	21.2744
45/−45/PZT	1–1	11.0622	11.0378	11.0196	11.1691	11.1447	11.1264
	1–2	20.8132	20.7843	20.7627	21.0101	21.5381	20.9590
	2–1	21.2716	21.2419	21.2201	21.5677	20.9808	21.5164

Table 12
Non-dimensional frequencies of piezo-hygro-thermo-elastic plates ($a/b = 1$, $a/h = 10$, C–C–C–C, $R/a = \infty$)

Laminate	Mode order	Ω_e	Ω_{te}	Ω_{he}	Ω_{pe}	Ω_{pte}	Ω_{phe}
0/90/PZT	1–1	14.8304	14.7723	14.7288	15.0056	14.9483	14.9055
	1–2	26.5977	26.5215	26.4646	26.7589	26.6832	26.6267
	2–1	27.5165	27.4438	27.3896	27.8672	27.7957	27.7422
	2–2	36.1760	36.0893	36.0243	36.5069	36.4212	36.3569
45/−45/PZT	1–1	14.4399	14.3810	14.3368	14.6134	14.5553	14.5117
	1–2	26.2379	26.1613	26.1038	26.4566	26.3806	26.3237
	2–1	26.6774	26.6026	26.5466	26.9941	26.9203	26.8651
	2–2	37.2473	37.1626	37.0994	37.5424	37.4585	37.3959

(simply supported shells: $\bar{\Omega}_{pe} \approx 5$–$6\%$; clamped shells: $\bar{\Omega}_{pe} \approx 5\%$). And this trend is observed to be the same both in $R_x/a = 10$ and $R_x/a = 5$. The piezoelectric actuation modelled in the present study is basically isotropic in nature ($d_{31} = d_{32}$). It is evident from the results that the isotropic actuation efficiently compensates the reduction in natural frequencies due to hygral and thermal

Table 13
Non-dimensional frequencies of piezo-hygro-thermo-elastic cylindrical shell ($a/b = 1$, $a/h = 100$, S–S–S–S, $R_x/a = 10$)

Laminate	Mode order	Ω_e	Ω_{te}	Ω_{he}	Ω_{pe}	Ω_{pte}	Ω_{phe}
0/90/PZT	1–1	10.2211	9.5971	9.0144	10.9434	10.1783	10.4890
	1–2	21.5817	20.7212	19.9626	22.9599	22.0240	21.8336
	2–1	26.7430	26.1177	25.5818	28.5248	27.8383	28.8501
	2–2	35.7179	34.5876	33.7201	38.0020	36.9973	37.3464
	1–3	40.4067	39.5262	38.7516	42.7379	41.7431	41.4023
45/−45/PZT	1–1	14.4642	13.7795	13.1030	15.3621	14.0521	13.3867
	1–2	23.0722	22.0225	21.0043	24.4039	21.9898	20.8356
	2–1	27.2787	26.3564	25.5358	29.1365	27.3812	26.5408
	1–3	39.0511	37.8609	36.7448	41.3217	38.9585	37.7690
	2–2	46.3052	45.4736	44.7293	49.0115	46.9869	46.2044

Table 14
Non-dimensional frequencies of piezo-hygro-thermo-elastic cylindrical shell ($a/b = 1$, $a/h = 100$, C–C–C–C, $R_x/a = 10$)

Laminate	Mode order	Ω_e	Ω_{te}	Ω_{he}	Ω_{pe}	Ω_{pte}	Ω_{phe}
0/90/PZT	1–1	24.5242	22.9637	22.011	25.7293	23.6138	22.2781
	1–2	35.1734	32.0191	30.0609	37.1028	33.6387	31.4675
	2–1	41.1288	39.3794	38.344	43.8669	40.7736	38.8802
	2–2	51.7259	48.8281	47.0946	54.8555	51.1248	48.8558
	1–3	55.7654	51.8213	49.4299	58.7585	54.6329	52.1280
45/−45/PZT	1–1	22.0049	20.2891	19.2277	23.2283	20.7036	19.0316
	1–2	34.2459	31.627	30.0079	36.1709	32.1593	29.5731
	2–1	38.2399	35.8938	34.4924	40.6949	37.3083	35.2036
	1–3	51.7210	48.8396	47.1129	54.6819	50.5913	48.0778
	2–2	61.4327	58.4724	56.6953	64.9663	60.7717	58.2240

Table 15
Non-dimensional frequencies of piezo-hygro-thermo-elastic cylindrical shell ($a/b = 1$, $a/h = 10$, S–S–S–S, $R_x/a = 10$)

Laminate	Mode order	Ω_e	Ω_{te}	Ω_{he}	Ω_{pe}	Ω_{pte}	Ω_{phe}
0/90/PZT	1–1	8.4221	8.4106	8.4021	8.5663	8.5537	8.5452
	1–2	19.8830	19.8682	19.8576	20.0518	20.0367	20.0261
	2–1	20.9780	20.9648	20.9552	21.3646	21.3511	21.3422
45/−45/PZT	1–1	11.1063	11.0821	11.0640	11.2189	11.1944	11.1762
	1–2	20.8029	20.7743	20.7530	21.0043	20.9749	20.9530
	2–1	21.2973	21.2675	21.2456	21.5986	21.5687	21.5469
	2–2	33.7128	33.6803	33.6564	33.9917	33.9585	33.9343

Table 16
Non-dimensional frequencies of piezo-hygro-thermo-elastic cylindrical shell ($a/b = 1$, $a/h = 10$, C–C–C–C, $R_x/a = 10$)

Laminate	Mode order	Ω_e	Ω_{te}	Ω_{he}	Ω_{pe}	Ω_{pte}	Ω_{phe}
0/90/PZT	1–1	14.9880	14.9312	14.8887	15.1668	15.1102	15.0679
	1–2	26.6595	26.5839	26.5275	26.8285	26.7532	26.6969
	2–1	27.5778	27.5065	27.4533	27.9288	27.8573	27.8038
	2–2	36.2207	36.1349	36.0706	36.5547	36.4689	36.4046
	1–3	42.7634	42.6728	42.6054	42.9373	42.8469	42.7797
45/−45/PZT	1–1	14.5359	14.4779	14.4345	14.7139	14.6562	14.6128
	1–2	26.2307	26.1550	26.0982	26.4534	26.3773	26.3204
	2–1	26.7436	26.6696	26.6142	27.0663	26.9924	26.9370
	2–2	37.2728	37.1890	37.1265	37.5732	37.4891	37.4265
	2–2	41.7131	41.6218	41.5533	42.0770	41.9854	41.9167

Table 17
Non-dimensional frequencies of piezo-hygro-thermo-elastic cylindrical shell ($a/b = 1$, $a/h = 100$, S-S-S-S, $R_x/a = 5$)

Laminate	Mode order	Ω_e	Ω_{te}	Ω_{he}	Ω_{pe}	Ω_{pte}	Ω_{phe}
0/90/PZT	1–1	14.7720	14.5298	14.2465	15.5252	14.4497	14.3868
	2–1	27.0027	26.6248	26.2206	28.9204	26.7141	26.8611
	1–2	28.7979	28.3787	27.9317	30.3507	29.4176	29.1242
	2–2	36.2489	35.3667	34.6145	38.8044	36.9035	36.6940
	1–3	47.0872	46.6048	46.0737	49.8527	48.8421	48.4137
45/−45/PZT	1–1	22.4581	22.2569	22.0122	23.5668	22.7038	20.9833
	2–1	24.1425	23.6517	23.1145	25.6501	22.4773	22.0877
	1–2	34.7796	34.4249	34.0308	36.8674	35.2791	34.4516
	1–3	42.1881	41.5970	40.9351	44.6908	41.7842	40.2686
	2–2	47.7948	47.3497	46.8995	50.7047	48.0875	46.8949

Table 18
Non-dimensional frequencies of piezo-hygro-thermo-elastic cylindrical shell ($a/b = 1$, $a/h = 100$, C-C-C-C, $R_x/a = 5$)

Laminate	Mode order	Ω_e	Ω_{te}	Ω_{he}	Ω_{pe}	Ω_{pte}	Ω_{phe}
0/90/PZT	1–1	37.8102	37.0379	36.5844	39.2567	37.6666	36.6786
	2–1	41.9351	40.9668	40.4021	44.7028	41.5182	39.5582
	1–2	45.8697	43.7034	42.4123	48.1135	45.3463	43.6576
	2–2	53.5618	51.3529	50.0489	56.8600	53.1522	50.8958
	1–3	63.4776	60.2148	58.2710	66.9757	63.2834	61.0655
45/−45/PZT	1–1	32.3819	31.6419	31.2066	33.8727	31.8426	30.4944
	2–1	38.1589	36.9385	36.2070	40.2014	36.3850	33.9366
	1–2	43.7662	42.1935	41.2780	46.4506	43.3122	41.3724
	1–3	55.6853	53.9099	52.8613	58.9297	54.9761	52.5695
	2–2	63.1547	61.3315	60.2127	66.8202	62.5619	59.9650

Table 19
Non-dimensional frequencies of piezo-hygro-thermo-elastic cylindrical shell ($a/b = 1$, $a/h = 10$, S–S–S–S, $R_x/a = 5$)

Laminate	Mode order	Ω_e	Ω_{te}	Ω_{he}	Ω_{pe}	Ω_{pte}	Ω_{phe}
0/90/PZT	1–1	8.4884	8.4772	8.4688	8.6362	8.6226	8.6138
	1–2	19.9581	19.9431	21.0113	20.1336	20.1179	20.1071
	2–1	21.0334	21.0207	19.9323	21.4219	21.4076	21.3988
45/−45/PZT	1–1	11.2566	11.2334	11.2159	11.3744	11.3496	11.3313
	1–2	20.8244	20.7967	20.7759	21.0302	20.9997	20.9773
	2–1	21.3757	21.3466	21.3251	21.6814	21.6507	21.6283

Table 20
Non-dimensional frequencies of piezo-hygro-thermo-elastic cylindrical shell ($a/b = 1$, $a/h = 10$, C–C–C–C, $R_x/a = 5$)

Laminate	Mode order	Ω_e	Ω_{te}	Ω_{he}	Ω_{pe}	Ω_{pte}	Ω_{phe}
0/90/PZT	1–1	15.4641	15.4109	15.3711	15.6447	15.5900	15.5491
	1–2	26.9069	26.8330	26.7778	27.0836	27.0090	26.9534
	2–1	27.6306	27.5631	27.5128	27.9813	27.9096	27.8559
	2–2	36.2787	36.1953	36.1328	36.6151	36.5293	36.4649
	1–3	42.8992	42.8096	42.7430	43.0822	42.9922	42.9253
45/−45/PZT	1–1	14.8274	14.7723	14.7310	15.0090	14.9522	14.9095
	1–2	26.2828	26.2097	26.1549	26.5090	26.4327	26.3756
	2–1	26.8736	26.8020	26.7483	27.2019	27.1277	27.0721
	2–2	37.3518	37.2704	37.2098	37.6570	37.5729	37.5102
	2–2	41.7350	41.6465	41.5800	42.1009	42.0088	41.9396

effects on cross-ply laminates, and moderately controls the dynamics of angle-ply laminate for $R_x/a = 10$. However, the performance of actuator lamina reduces drastically in the case of $R_x/a = 5$ for cross-ply laminate and does not seem to be effective in angle-ply laminate. Therefore, to achieve better structural control of a moderately thin laminate that has the extension-bending and extension-twisting coupling, it is essential to tailor the piezoelectric actuation along the fibre direction using the directional actuators (*P*iezo*F*ibre *C*omposites, *A*ctive *F*ibre *C*omposites, *D*irectionally *A*ctive *P*iezos). In the case of cylindrical shells with $a/h = 10$, the boundary effect does not seem to influence the active stiffening and active compensation is very low independent of boundary conditions.

5.2.3. *Active stiffening and active compensation effects on spherical shells*

The spherical cross-ply and angle-ply laminated shells with R_x/a, $R_y/a = 10$ and 5 are taken to study the stiffening effect on the frequency control and the results are given in Tables 21–28. A moderate reduction in natural frequencies is observed due to hygral and thermal effects. The active stiffening is relatively efficient in the simply supported shells ($\bar{\Omega}_{pe} \approx 6\%$ for R_x/a, $R_y/a = 10$) than the clamped shells ($\bar{\Omega}_{pe} \approx 5.5\%$). However, in the case of R_x/a, $R_y/a = 5$, the active stiffening

Table 21
Non-dimensional frequencies of piezo-hygro-thermo-elastic spherical shell ($a/b = 1$, $a/h = 100$, S–S–S–S, $R_x/a = 10$, $R_y/a = 10$)

Laminate	Mode order	Ω_e	Ω_{te}	Ω_{he}	Ω_{pe}	Ω_{pte}	Ω_{phe}
0/90/PZT	1–1	14.7851	14.5585	14.2862	15.5401	14.7274	14.8041
	2–1	22.9975	22.4827	21.9488	24.4402	22.7582	22.7712
	1–2	29.7159	29.3991	29.0298	31.9276	30.5495	30.5011
	2–2	36.2493	35.4355	34.7159	38.8058	36.9668	36.7990
	1–3	40.9263	40.3780	39.8011	43.3181	41.4656	41.5864
45/−45/PZT	1–1	22.4796	22.2801	22.0364	23.5909	22.5910	22.0843
	1–2	26.6311	26.2049	25.6803	28.3164	25.8609	24.5220
	2–1	29.7049	29.2720	28.8436	31.7655	29.6782	28.6549
	1–3	41.9556	41.3501	40.6599	44.5750	41.8096	40.3294
	2–2	46.7400	46.3208	45.8721	49.8078	47.1806	45.9656

Table 22
Non-dimensional frequencies of piezo-hygro-thermo-elastic spherical shell ($a/b = 1$, $a/h = 100$, C–C–C–C, $R_x/a = 10$, $R_y/a = 10$)

Laminate	Mode order	Ω_e	Ω_{te}	Ω_{he}	Ω_{pe}	Ω_{pte}	Ω_{phe}
0/90/PZT	1–1	30.7714	30.2691	29.9767	32.5210	30.6465	29.4119
	1–2	35.6555	34.6115	33.9995	37.6824	33.9624	31.5715
	2–1	45.6022	44.7078	44.1876	48.9187	46.0205	44.2393
	1–3	52.6109	51.0507	50.1414	56.0362	52.2008	49.8456
	2–2	56.4508	55.2200	54.4990	59.5392	55.2055	52.5688
45/−45/PZT	1–1	29.3912	28.8276	28.4980	31.0011	28.8291	27.3665
	1–2	37.1569	36.0090	35.3360	43.5895	35.3303	32.7108
	2–1	40.8865	39.8392	39.2248	39.3612	40.1654	38.0204
	2–2	54.5300	53.1033	52.2724	57.8398	53.7027	51.1617
	1–3	61.8338	60.2830	59.3762	65.6541	61.1054	58.3100

Table 23
Non-dimensional frequencies of piezo-hygro-thermo-elastic spherical shell ($a/b = 1$, $a/h = 10$, S–S–S–S, $R_x/a = 10$, $R_y/a = 10$)

Laminate	Mode order	Ω_e	Ω_{te}	Ω_{he}	Ω_{pe}	Ω_{pte}	Ω_{phe}
0/90/PZT	1–1	8.4573	8.4457	8.4371	8.6049	8.5929	8.5848
	1–2	19.8298	19.8145	19.8035	19.9998	19.9844	19.9744
	2–1	21.0025	20.9896	20.9801	21.3972	21.3833	21.3741
45/−45/PZT	1–1	11.2786	11.2554	11.2380	11.3967	11.3720	11.3537
	1–2	20.8150	20.7873	20.7665	21.0210	20.9906	20.9682
	2–1	21.3426	21.3134	21.2919	21.6487	21.6178	21.5954

Table 24
Non-dimensional frequencies of piezo-hygro-thermo-elastic spherical shell ($a/b = 1$, $a/h = 10$, C–C–C–C, $R_x/a = 10$, $R_y/a = 10$)

Laminate	Mode order	Ω_e	Ω_{te}	Ω_{he}	Ω_{pe}	Ω_{pte}	Ω_{phe}
0/90/PZT	1–1	15.1759	15.1217	15.0811	15.3625	15.3067	15.2650
	1–2	26.5950	26.5223	26.4680	26.7647	26.6889	26.6324
	2–1	27.7111	27.6420	27.5903	28.0749	28.0035	27.9501
	2–2	36.1829	36.0994	36.0369	36.5201	36.4341	36.3696
	1–3	42.6949	42.6079	42.5433	42.8691	42.7784	42.7109
45/−45/PZT	1–1	14.7555	14.7002	14.6587	14.9379	14.8808	14.8380
	1–2	26.2540	26.1807	26.1259	26.4807	26.4043	26.3471
	2–1	26.8386	26.7671	26.7134	27.1670	27.0928	27.0371
	2–2	37.3354	37.2539	37.1933	37.6407	37.5565	37.4938
	2–2	41.7157	41.6270	41.5606	42.0825	41.9903	41.9211

Table 25
Non-dimensional frequencies of piezo-hygro-thermo-elastic spherical shell ($a/b = 1$, $a/h = 100$, S–S–S–S, $R_x/a = 5$, $R_y/a = 5$)

Laminate	Mode order	Ω_e	Ω_{te}	Ω_{he}	Ω_{pe}	Ω_{pte}	Ω_{phe}
0/90/PZT	1–1	26.8985	26.8583	26.7950	27.6751	26.9552	26.7622
	1–2	33.5011	33.3124	33.1123	35.0940	33.3540	32.7679
	2–1	38.8524	38.7598	38.5946	41.2471	39.6423	39.0784
	2–2	40.8525	40.3832	39.9597	43.7283	41.3866	40.5431
	1–3	49.1120	48.8677	48.6027	51.9443	49.5109	48.7239
45/−45/PZT	1–2	38.6166	38.5171	38.3407	40.5408	38.6663	37.6246
	2–1	40.9612	40.7893	40.6190	42.5143	41.4899	40.6141
	1–1	41.0132	40.9719	40.9044	43.2732	41.8769	41.4684
	1–3	50.6756	50.5082	50.2249	53.8075	50.9988	49.4808
	2–2	51.8227	51.6548	51.4437	55.3330	52.5531	51.1393

Table 26
Non-dimensional frequencies of piezo-hygro-thermo-elastic spherical shell ($a/b = 1$, $a/h = 100$, C–C–C–C, $R_x/a = 5$, $R_y/a = 5$)

Laminate	Mode order	Ω_e	Ω_{te}	Ω_{he}	Ω_{pe}	Ω_{pte}	Ω_{phe}
0/90/PZT	1–2	48.0811	47.8948	47.7844	50.4500	47.6006	45.8264
	1–1	51.5383	51.4765	51.4390	54.0567	52.0471	50.6701
	2–1	56.1802	55.9227	55.7704	59.8344	57.2103	55.5801
	2–2	58.2006	57.5249	57.1383	61.9543	58.4337	56.2913
	1–3	67.1440	66.8896	66.7360	70.8518	67.6127	65.7642
45/−45/PZT	1–1	48.9962	48.7660	48.6004	51.3692	48.4137	46.4296
	1–2	49.0499	48.9223	48.8759	51.5689	49.0617	47.4823
	2–1	52.0116	51.7004	51.5191	55.0240	52.1831	50.4312
	1–3	65.9500	65.5640	65.1903	69.8197	66.1228	63.4793
	2–2	66.2055	65.4797	65.2066	70.4439	66.6029	64.7215

Table 27
Non-dimensional frequencies of piezo-hygro-thermo-elastic spherical shell ($a/b = 1$, $a/h = 10$, S–S–S–S, $R_x/a = 5$, $R_y/a = 5$)

Laminate	Mode order	Ω_e	Ω_{te}	Ω_{he}	Ω_{pe}	Ω_{pte}	Ω_{phe}
0/90/PZT	1–1	8.7215	8.7107	8.7026	8.8730	8.8589	8.8499
	1–2	19.8883	19.8728	19.8617	20.0658	20.0464	20.0344
	2–1	21.1880	21.1764	21.1675	21.5904	21.5737	21.5631
45/−45/PZT	1–1	11.9397	11.9200	11.9050	12.0667	12.0415	12.0229
	1–2	20.9458	20.9211	20.9025	21.1598	21.1260	21.1012
	2–1	21.5365	21.5100	21.4902	21.8506	21.8164	21.7916

Table 28
Non-dimensional frequencies of piezo-hygro-thermo-elastic spherical shell ($a/b = 1$, $a/h = 10$, C–C–C–C, $R_x/a = 5$, $R_y/a = 5$)

Laminate	Mode order	Ω_e	Ω_{te}	Ω_{he}	Ω_{pe}	Ω_{pte}	Ω_{phe}
0/90/PZT	1–1	16.1541	16.1092	16.0757	16.3496	16.2973	16.2583
	1–2	26.7797	26.7161	26.6687	26.9574	26.8817	26.8252
	2–1	28.0822	28.0219	27.9769	28.4566	28.3855	28.3323
	2–2	36.2410	36.1658	36.1096	36.5834	36.4968	36.4318
	1–3	42.7827	42.706	42.6491	42.9665	42.8755	42.8079
45/−45/PZT	1–1	15.6746	15.6283	15.5936	15.8636	15.8093	15.7685
	1–2	26.4531	26.3886	26.3403	26.6868	26.6096	26.5518
	2–1	27.1773	27.1144	27.0672	27.5153	27.4403	27.3841
	2–2	37.6026	37.5297	37.4754	37.9174	37.8330	37.7701
	2–2	41.7601	41.6808	41.6213	42.1321	42.0379	41.9672

is found to be better in clamped shells. It is also noticed that the piezoelectric actuation trend in controlling the frequency is same for both cross-ply and angle-ply laminates. The active compensation by piezoelectric actuator is observed to be relatively lower in thin piezo-hygro-thermo-elastic spherical shells compared to thin plates and cylindrical shells. In the case of spherical shells with $a/h = 10$, the active stiffening and active compensation effects are very low independent of boundary conditions.

6. Conclusions

A generalized FE formulation involving electromechanical coupling and hygrothermal strain field is presented. Further, a nine-noded field consistent Langrangian element is developed to study the influence of active stiffening on the frequency control of piezo-hygro-thermo-elastic laminated plates and shells. The hygrothermal strain modifies the elastic stiffness and brings down the elastic frequencies of piezoelectric laminated plates and shells significantly. The isotropic PZT actuator modelled in the present formulation actively compensates the frequency reduction that

has occurred due to hygral and thermal effects in cross-ply laminates. However, it is observed that the actuator performance reduces significantly with increase in curvature particularly in angle-ply laminates, which demands the use of directional actuators. The active stiffening and active compensation effects are low in moderately thick piezo-hygro-thermo-elastic plates and shells, which are less influenced by boundary conditions.

Appendix A. Notation

a, b	side length in x and y directions, respectively
E_x, E_y, E_z	electric field in x, y and z axes, respectively
$\varepsilon_m, \varepsilon_b, \varepsilon_s$	strains due to membrane, bending and shear, respectively
e_1, e_2	non-mechanical strains due temperature and moisture
d_{31}, d_{32}	piezoelectric constants with respect to 1 and 2 axes
$\kappa_{11}, \kappa_{22}, \kappa_{33}$	di-electric constants with respect to 1, 2 and 3 axes
Ω_e	non-dimensional frequency of elastic system
Ω_{te}	non-dimensional frequency of thermoelastic system
Ω_{he}	non-dimensional frequency of hygroelastic system
Ω_{pe}	non-dimensional frequency of piezoelectric system
Ω_{pte}	non-dimensional frequency of piezo-thermo-elastic system
Ω_{phe}	non-dimensional frequency of piezo-hygro-elastic system
$\bar{\Omega}_e$	$= \left(\frac{\Omega_e - \Omega_{te}}{\Omega_e}\right) \times 100, = \left(\frac{\Omega_e - \Omega_{he}}{\Omega_e}\right) \times 100$
$\bar{\Omega}_e$	reduction in non-dimensional frequency due hygrothermal effect
$\bar{\Omega}_{pe}$	$= \left(\frac{\Omega_{pe} - \Omega_e}{\Omega_{pe}}\right) \times 100$
$\bar{\Omega}_{pe}$	active stiffening through actuation
$\bar{\Omega}_{pte}$	$= \left(\frac{\Omega_{pte} - \Omega_{te}}{\Omega_{pte}}\right) \times 100$
$\bar{\Omega}_{pte}$	active compensation through actuation (piezo-thermo-elastic)
$\bar{\Omega}_{phe}$	$= \left(\frac{\Omega_{phe} - \Omega_{he}}{\Omega_{phe}}\right) \times 100$
$\bar{\Omega}_{phe}$	active compensation through actuation (piezo-hygro-elastic)
$\Omega_{(e,he,te,pe,pte,phe)}$	$= \omega_{(e,he,te,pe,pte,phe)} a^2 \sqrt{\rho/E_2}/h$
$\omega_{(e,he,te,pe,pte,phe)}$	natural frequency of the system

References

[1] H.S. Tzou, R. Ye, Piezothermoelasticity and precision control of piezoelectric systems: theory and finite element analysis, *Journal of Vibration and Acoustics* 116 (1994) 489–495.

[2] H.J. Lee, D.A. Saravanos, Coupled layer-wise analysis of thermo-piezoelectric composite beams, *American Institute of Aeronautics and Astronautics Journal* 34 (6) (1996) 1231–1237.

[3] S. Raja, K. Rohwer, M. Rose, Piezothermoelastic modelling and active vibration control of laminated piezoelectric composite beam, *Journal of Intelligent Material Systems and Structures* 10 (11) (1999) 890–899.
[4] K.D. Jonnalagadda, G.E. Blandford, T.R. Tauchert, Piezothermoelastic composite plate analysis using first order shear deformation theory, *Computers and Structures* 51 (1) (1994) 79–89.
[5] G.E. Blandford, T.R. Tauchert, Y. Du, Self-strained piezothermoelastic composite beam analysis using first order shear deformation theory, *Composites: Part B* 30 (1999) 51–63.
[6] K. Chandrashekhara, M. Kolli, Thermally induced vibration of adaptive doubly curved composite shells with piezoelectric devices, in: *Proceedings of the 36th AIAA/ASME/ASCE/AHS/ASC Structures, Structural Dynamics and Materials Conference*, New Orleans, LA, April 10–13, AIAA-95-1352-CP, 1995, pp. 1628–1629.
[7] H.J. Lee, D.A. Saravanos, A mixed multi-field finite element formulation for thermopiezoelectric composite shells, *International Journal of Solids and Structures* 37 (2000) 4949–4967.
[8] Z. Xu, A. Chattopadhyay, H. Gu, Dynamic response of smart composites using a coupled thermo-piezoelectric-mechanical model, *American Institute of Aeronautics and Astronautics Journal* 38 (10) (2000) 1939–1948.
[9] M. Ishihara, N. Noda, Dynamic behaviour of a peizothermoelastic laminate considering the effect of transverse shear, *Smart Materials and Structures* 11 (2002) 202–208.
[10] H.S. Tzou, Y.H. Zhou, Nonlinear piezothermoelasticity and multi-field actuations, Part 2: control of nonlinear deflection buckling, and dynamics, *Journal of Vibration and Acoustics* 119 (3) (1997) 382–389.
[11] Y. Bao, H.S. Tzou, V.B. Venkayya, Analysis of nonlinear piezothermoelastic laminated beams with electric and temperature effects, *Journal of Sound Vibration* 209 (3) (1998) 505–518.
[12] I.K. Oh, J.H. Han, In. Lee, Postbuckling and vibration characteristics of piezolaminated composite subject to thermopiezoelectric loads, *Journal of Sound Vibration* 233 (1) (2000) 19–40.
[13] I.K. Oh, J.H. Han, In. Lee, Thermopiezoelastic snapping of piezolaminated plates using layerwise nonlinear finite elements, *American Institute of Aeronautics and Astronautics Journal* 39 (6) (2001) 1188–1197.
[14] S. Shen, Z.B. Kuang, An active control model of laminated piezothermoelastic plate, *International Journal of Solids and Structures* 36 (1999) 1925–1947.
[15] S.Y. Lee, W.J. Yen, Hygrothermal effects on the stability of a cylindrical composite shell panel, *Computers and Structures* 33 (2) (1989) 551–559.
[16] J.N. Reddy, Exact solutions of moderately thick laminated shells, *Journal of Engineering Mechanics—American Society of Civil Engineers* 110 (1984) 794–809.
[17] P. Bhattacharya, H. Suhail, P.K. Sinha, Finite element free vibration analysis of smart laminated composite beams and plates, *Journal of Intelligent Material Systems and Structures* 9 (1) (1998) 20–29.
[18] M.C. Ray, R. Bhattacharya, B. Samanta, Exact solutions for static analysis of intelligent structures, *American Institute of Aeronautics and Astronautics Journal* 31 (9) (1994) 1684–1691.
[19] K.S. Sai Ram, P.K. Sinha, Hygrothermal effects on the free vibration of laminated composite plates, *Journal of Sound Vibration* 158 (1) (1992) 133–148.
[20] E. Carrera, An assessment of mixed and classical theories on global and local response of multilayered orthotropic plates, *Composite Structures* 50 (2) (2000) 183–198.
[21] A. Nosier, R.K. Kapania, J.N. Reddy, Free vibration analysis of laminated plates using a layerwise theory, *American Institute of Aeronautics and Astronautics Journal* 31 (12) (1993) 2335–2346.
[22] K.R. Thangaratnam, Palaninathan, J. Ramachandran, Thermal buckling of composite laminated plates, *Computer and Structures* 32 (1989) 1117–1124.